

# Leveraging Bitstream Metadata for Fast and Accurate Video Compression Correction

Max Ehrlich<sup>1,2</sup>, Jon Barker<sup>2</sup>, Namitha Padmanabhan<sup>1</sup>, Larry Davis<sup>1</sup>, Andrew Tao<sup>2</sup>, Bryan Catanzaro<sup>2</sup>, Abhinav Shrivastava<sup>1</sup>

<sup>1</sup>University of Maryland <sup>2</sup>NVIDIA

{maxehr, lsd}@umiacs.umd.edu {jbarker, atao, bcatanzaro}@nvidia.com namithap@umd.edu abhinav@cs.umd.edu

## Abstract

*Video compression is a central feature of the modern internet powering technologies from social media to video conferencing. While video compression continues to mature, for many, and particularly for extreme, compression settings, quality loss is still noticeable. These extreme settings nevertheless have important applications to the efficient transmission of videos over bandwidth constrained or otherwise unstable connections. In this work, we develop a deep learning architecture capable of restoring detail to compressed videos which leverages the underlying structure and motion information embedded in the video bitstream. We show that this improves restoration accuracy compared to prior compression correction methods and is competitive when compared with recent deep-learning-based video compression methods on rate-distortion while achieving higher throughput.*

## 1. Introduction

At its conception, the internet was a medium for the exchange of text data. This has rapidly changed over the last decade to focus on multimedia, and in particular, video [1], [2]. Video compression is, therefore, a critical feature of the modern internet. Even short videos are orders of magnitude larger than text data in their uncompressed form and would be impossible to transmit in a timely manner over even a broadband connection.

Although modern block-based codecs [3]–[7] are able to achieve impressive compression ratios with limited quality loss, even these codecs are challenged by bandwidth-limited scenarios which are common in third world countries, rural locations, and lower-class households [8]. Moreover, the additional transmission latency induced by a low-bandwidth internet connection is unstable: effective bandwidth can vary greatly over time. One way to overcome this limitation is to increase the aggressiveness of the video encoder creating a smaller transmission, however this comes with an asso-



Figure 1. **Don’t Spend Megabits, Use MetaBit.** Our MetaBit system takes heavily compressed frames and restores detail. The above example is stored at only 0.039bpp. For each pair, our restoration is shown with a **blue** border. Our method is able to faithfully restore natural textures (**left trees**), clothing textures/human appearance (**middle woman**), and artificial textures (**top roof**).

ciated loss in visual fidelity. We solve this fidelity loss by formulating MetaBit, a novel convolutional neural network architecture [9], [10] for restoring compressed videos. An example of this is shown in Figure 1. In effect, we are trading off the unpredictable and often extreme latency of internet transmission for the measurable and predictable latency of deep learning.

This particular restoration problem is understudied [11]–[13] when compared with tasks like super-resolution, and we identified several problems in prior art. Firstly, prior works expend significant resources on either explicit [11], [13] or implicit [12] motion estimation. Secondly, although Yang *et al.* [11] correctly observe that not all frames contain the same amount of information, they rely on explicit supervision, and

train a discriminative model, to determine the frames with the most information which makes training cumbersome. Finally, prior works received limited evaluation, using only the H.265 (HEVC) [5] compression algorithm with constant QP compression (see Section 3 for a detailed discussion). Although H.265 is an exciting modern codec it is underutilized with H.264 (AVC) covering many more videos [1], and the degradations H.265 causes are less noticeable. Moreover, the constant QP setting is rarely used in real videos.

In contrast, our formulation leverages the underlying structure and motion embedded in the compressed bitstream for both a higher fidelity reconstruction and faster throughput and we evaluate our method (and prior works) on more realistic data. Modern block-based codecs include their own coarse motion estimation in the form of *Motion Vectors*. Our network leverages these motion vectors to perform coarse motion compensation without the need for any additional computation. Additionally, modern codecs compact information into *Intra-Frames* (I-frames) with later *Predicted-Frames* (P-frames) providing only residual data. We leverage these I-frames as high-information-content frames and use their representation to guide enhancement of the low-information P-frames. This allows us to allocate more parameters to the I-frames and less parameters to the P-frames consequently accelerating the entire architecture. This also introduces a new restoration paradigm: where prior works are sliding-window methods which take a group of frames and produce a single output frame, our method restores blocks of frames at a time, *i.e.*, in a single forward pass, our network consumes 7 degraded frames and predicts 7 high quality frames. This paradigm is much faster than the sliding window methods. Note that despite leveraging the bitstream in this way, our method is *codec-agnostic*: it uses information contained in every modern video codec.

Although we show state-of-the-art results under the same conditions as prior works, we additionally test using the more common H.264 codec [3] in both “common” and “extreme” settings (see Section 5.4). We find that while deep networks are able to improve the quality of extremely compressed frames, they require additional supervision to do so. In particular, we formulate a *Scale-Space* [14] loss that allows the network to focus on high frequency details which are removed by compression and we use a GAN [15] loss which enables the network to hallucinate plausible reconstructions. We additionally compare our method to fully deep-learning-based compression codecs and find that simply using H.264, a widely supported codec, with our restoration network is competitive in terms of rate-distortion and decoding time.

In summary, our primary contributions are:

1. An extremely efficient formulation for video compression correction which leverages the underlying bitstream structure of compressed videos to achieve state-of-the-art performance.



Figure 2. **Motion Vectors.** Motion vectors resemble downsampled optical flow. Left: reference image. Middle: optical flow. Right: motion vectors extracted from the video bitstream. Optical flow was computed with RAFT [16].

2. A more rigorous evaluation procedure which includes tests on realistic and extreme compression settings.
3. Improved loss formulations which allow the network to produce plausible reconstructions in extreme compression scenarios.

## 2. Prior Work

**JPEG Artifact Correction** The related problem of JPEG [17] artifact correction is a rich area of study with consistent progress each year. In recent years this problem is solved using convolutional neural networks [9], [10]. ARCNN [18] is the first such method which was a simple regression technique inspired by super-resolution architectures. This work was continued with the L4, L8, and CAS-CNN [19], [20] methods. These works were later extended to “dual-domain” methods [21]–[25]. One flaw in these works was their focus on “quality-aware” formulations, in other words. This was solved by Ehrlich *et al.* [26], [27] using a formulation which was conditioned on the JPEG quantization matrix and later improved by Jiang *et al.* [28] where the network was encouraged to correctly predict the JPEG quality.

**Video Restoration** Video compression correction is directly related to other video restoration tasks. Toflow [29] used optical flow which is trained end-to-end with the restoration task to align frames and operated as a sliding window. EDVR [30] also operates as a sliding window but replaces the explicit motion estimation with deformable convolutions [31]. Jo *et al.* [32] propose a super-resolution method based on learned upsampling kernels rather than direct prediction. Chan *et al.* [33] analyze critical components of super-resolution and use this to design a simple, flexible architecture. Relevant here, Li *et al.* [34] consider super-resolution with common video compression settings.

**Video Compression Correction** Video compression correction, the task we solve here, was initially solved using

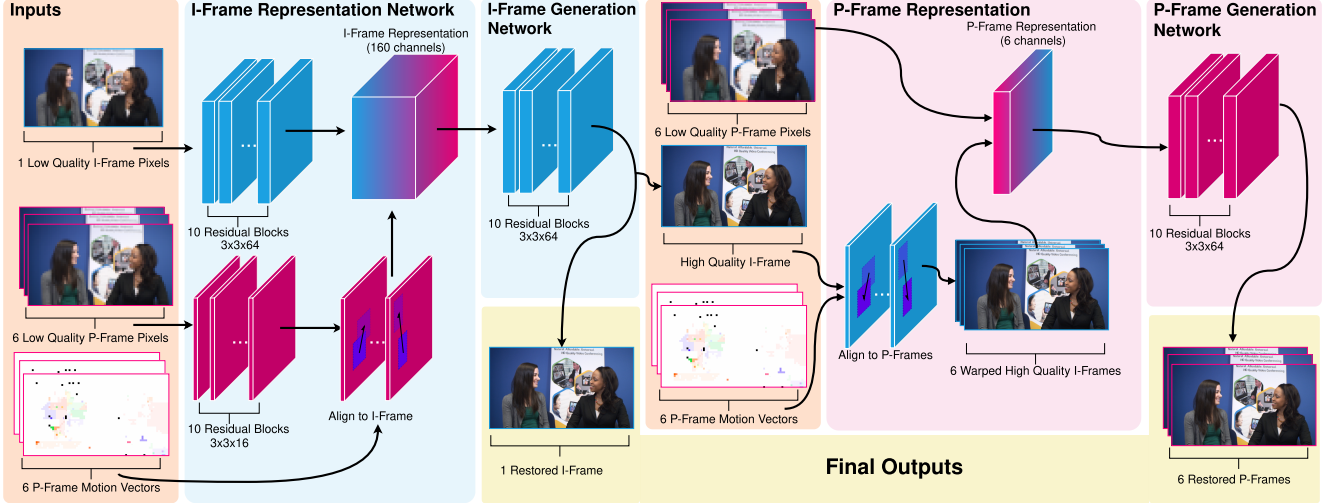


Figure 3. **MetaBit System Overview.** I-Frames are shown in **Blue** and P-Frames are shown in **Pink**. Our network takes an input (**Orange**) in the form of a low-quality Group-of-Pictures and first performs multi-frame correction on the **I-Frame**. The resulting high-quality **I-Frame** is used to guide correction of the low-quality **P-Frames**. The final output of our network (**Yellow**) is the entire high-quality Group-of-Pictures.

“single-frame” enhancement methods [35], [36] which outperform image-based restoration techniques but use only a single frame at a time. Yang *et al.* [11] propose MFQE which takes multiple frames in a sliding window to correct an entire video sequence. In addition to being the first multi-frame video compression correction model, their key contribution is the concept of *Peak Quality Frames* (PQFs). These are individual frames that have a higher perceptual quality than other nearby frames, and they are identified using a manually trained SVM [37]. They combine information from nearby frames using pixel-wise motion estimation and warping. Xing *et al.* [13] extend this idea by replacing the PQF detecting SVM with a BiLSTM [38]. Deng *et al.* [12] use implicit motion compensation with deformable convolutions [31]. They show that this leads to a more accurate and faster formulation. More recently, Ding *et al.* [39] design an architecture for capturing adjacent patch information more effectively and Zhao *et al.* [40] use a recurrent hidden state and deformable attention to improve the corrected result. In contrast to these techniques, our method requires no motion estimation for alignment and no supervision to determine high-information frames.

### 3. Background

Our method leverages concepts from video compression to improve both processing speed and restoration quality over prior works. We begin by briefly reviewing these guiding first-principles. Note that while we have selected H.264 and H.265 for evaluations, our method depends on information found in all codecs and is equally applicable to VP8/9, AV1, *etc.*, and nothing presented in this section is codec specific.

**Group of Pictures** Modern video encoders compact information over time into a *Group of Pictures* (GOP) based

on the assumption that over a small time interval, motion, and therefore the difference between neighboring frames, is small. All modern codecs use the concepts of *Intra-frames* (I-frames) and *Predicted-frames* (P-frames), with MPEG codecs additionally defining *Bipredicted-frames* (B-frames). I-frames are similar to JPEG images and are so called because they can be decoded using information contained within the frame itself. P-frames require at least one previous frame to decode (they are *predicted* from a previous frame). B-frames require at least one previous **and future** frame to decode. For simplicity, we do not use B-frames although there is no reason they could not be incorporated into our architecture. P-frames contain two major components: *Motion Vectors* (discussed in the next section) and *Error Residuals*. After performing motion compensation on a prior frame, the error residuals are simply the difference image between the compensated frame and the true frame, and therefore encode all new information that could not be modeled by motion alone (as well as motion errors). As I-frames contain most of the information for a GOP, we allocate more parameters to the representation and generation of the high quality I-frame and use that result to guide restoration of the low-information P-frames.

**Motion Compensation** Video codecs include coarse heuristic motion estimation in the encoding process. As discussed in the previous section, this allows P-frames to encode only “new information” which cannot be modeled by motion alone. These motion vectors are computed on blocks of pixels. See Figure 2 for a visual comparison of motion vectors to optical flow. In H.264 [3], for example, these blocks can be of size  $16 \times 16$ ,  $16 \times 8$ ,  $8 \times 16$ , or  $8 \times 8$  pixels. This operation alone compresses blocks of pixels into 4 tuples of source and destination while also reducing the entropy of



the error residual. Our network uses these coarse motions for alignment in lieu of pixelwise flows which would need to be computed.

**Tuning Quality vs. Bitrate** Modern codecs provide several methods for tuning the perceptual quality of a video stream. By lowering the quality, the codec is able to further compress the stream resulting in a smaller file. The most common methods are *Constant Rate Factor* (CRF) and *Constant Bitrate* (CBR) with CRF being the default method in many implementations [41]. In the CRF paradigm, the user presents the encoder with an integer in  $[0, 51]$  where 0 is defined to be “truly lossless” encoding and  $1 - 51$  define increasingly lossy modes. The default value in ffmpeg is 25 [41], this mode is generally only noticeable on close inspection. Therefore, the CRF method is considered a “proxy” for perceptual quality much in the same way that a JPEG quality in  $0 - 100$  is. In CBR mode, the encoder is asked to target a specific bitrate in bits-per-second (BPS). This mode is commonly used if a stream is to be transmitted over a connection of known maximum bandwidth. However, it is difficult for the encoder to know *a priori* how to do this, therefore the encoder regularly over or undershoots its bitrate target in this mode unless “two-pass encoding” is used, which is naturally slower.

There exists a third method: *Constant Quantization Parameter* (CQP), this is the mode tested by prior works [11]–[13]. In both of the above cases, the encoder converts the user input (CRF or target bitrate) to a set of “QPs” which are used to quantize transform coefficients. These QPs generally vary over space and time based on the estimated information content of the frames. In CQP encoding, the user provides a single QP directly and the encoder uses it for all frames without regard for information content. Use of this method is generally discouraged in real scenarios since the codec is no longer making intelligent decisions about which information to keep or discard. However, this method is attractive for machine learning because a single QP incurs a predictable degradation. In contrast, varying QPs over space and time (as in CRF and CBR) incur different degradations even within the same frame. Since this mode is not used in real videos, we additionally study CRF, the most common compression method, in this paper.

## 4. Method

Our task is to take a compressed frame  $C$  and compute a restored network output  $O$  which is as close as possible to the target (uncompressed) frame  $T$ . We accomplish this with a novel multiframe restoration network and loss functions. One unique aspect of compression restoration, when compared to other problems such as denoising, is that we have an exact target frame and we know the exact procedure that was performed on the target frame which caused the degradation. This allows us to design a network architecture that

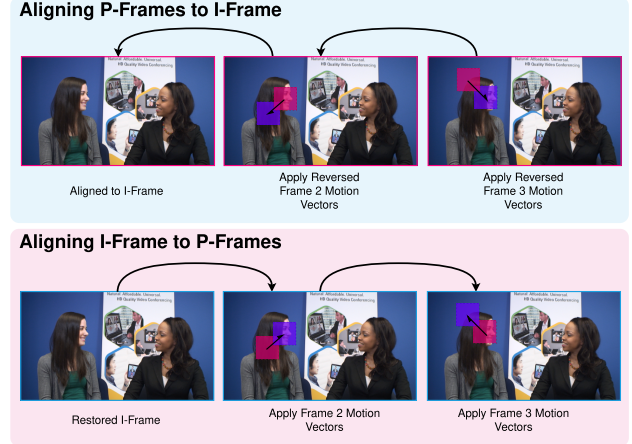


Figure 4. **Motion Compensation Example.** We use motion vectors from the video file to perform motion compensation both to align P-frames to the I-frame (top) and to align the restored I-frame to the P-frames (bottom). In the top example, the 3rd P-frame is aligned to the I-frame. Blocks of features are copied according to the reversed frame 3 motion vectors. This is repeated for frame 2’s motion vectors. The result is a feature map which is aligned to the I-frame. For P-frame alignment, the motion vectors are applied in the forward direction. In the bottom image, the I-frame is aligned to frames 2 and 3.

is informed by this procedure, and in our case, incorporate metadata contained in the compressed video bitstream.

In particular, multiframe restoration methods are known to improve when features in different frames are aligned (see Section 5.6 for an ablation of this). Rather than compute motion estimation, we leverage the motion vectors contained in the video bitstream. Additionally, video compression allocates more information to I-frames than to P-frames (Section 3). This was reflected in the “Peak-Quality Frames” of MFQE [11], [13] which required explicit supervision. Instead of computing the locations of these frames, our method simply assumes they are I-Frames<sup>1</sup>. By eliminating the need to perform explicit motion estimation and detect high quality reference frames, we can reinvest the requisite parameters directly in the restoration task leading to high quality results. In the remainder of this section we describe our novel restoration procedure and loss formulations. The procedure is shown graphically in Figure 3.

### 4.1. Restoration Procedure

**Modified ResBlock** As a standard building block for our network, we employ a modified version of the Residual Block [42] which is designed to perform better on restoration tasks. While a traditional Residual Block contains two Batch Normalization [43] layers, this is known to degrade

<sup>1</sup>Examining charts provided by Yang *et al.* [11] shows that the PQFs they detect are likely I-Frames due to their regular spacing, although we do not analyze this here.



Table 1. **Quantitative Evaluation.** We report  $\Delta$ PSNR (dB)  $\uparrow$  /  $\Delta$ LPIPS  $\downarrow$ , averaged over the MFQE [11] test split. We retrain STDF to report LPIPS on H.265. The H.265 evaluation is done in CQP mode to match prior works, for H.264 we use CRF for more realistic conditions.

Method	H.265 CQP			H.264 CRF			
	27	32	37	25	35	40	50
MFQE 1.0 [11]	0.40 / -	0.43 / -	0.46 / -	-	-	-	-
MFQE 2.0 [13]	0.49 / -	0.52 / -	0.56 / -	-	-	-	-
STDF-R1 [12]	0.59 / 0.027	0.64 / 0.028	0.65 / 0.034	0.741 / 0.034	0.862 / 0.032	0.814 / 0.030	0.632 / 0.013
STDF-R3 [12]	0.72 / <b>0.025</b>	0.86 / 0.027	0.83 / 0.033	0.784 / 0.035	0.846 / 0.032	0.882 / 0.029	0.817 / 0.011
<b>MetaBit (Ours)</b>	<b>1.17 / 0.025</b>	<b>0.99 / 0.023</b>	<b>0.91 / 0.029</b>	<b>1.085 / 0.024</b>	<b>1.137 / 0.014</b>	<b>1.113 / 0.005</b>	<b>0.887 / -0.016</b>

performance on restoration tasks [44]. Our residual blocks exclude batch norm, change ReLU for LeakyReLU, and include simple channel attention [45], [46] at the beginning of the block.

**I- and P-Frame Representations** Our network first performs a multi-frame restoration on I-frames. Since the I-frame itself contains most of the information in a group-of-pictures, we compute a 64-dimensional representation using 10 residual blocks. We then compute a 16-dimensional representation of the P-frames using 10 residual blocks. This process is shown in the top part of the blue box in Figure 3.

**Motion Vector Alignment** We then align the P-frame representations to the I-frame representation by warping the P-frame features using motion vectors (Figure 4 top). Each P-frame contains motion vectors that copy blocks of pixels from the previous frame into new locations in the destination frame. We reverse the direction of these vectors and copy the P-frame features backwards to align with the previous frame. Repeating this process for all motion vectors in the group-of-pictures yields a volume of P-frame features which are coarsely aligned with the I-frame.

**I-Frame Generation** We concatenate the I-frame features and aligned P-frame features channel-wise to yield a volume containing aligned features for the entire group-of-pictures. For a 7 frame GOP, this is a 160-dimensional representation which we project to 64 dimensions for efficiency. We then generate the high-quality I-frame using 10 more residual blocks with the final one yielding a 3 or 1 channel output.

**P-Frame Generation** Finally, we use the high-quality I-frame to generate the high-quality P-frames. Each I-frame is warped using the P-frame motion vectors to yield 6 copies of the I-frame (Figure 4 bottom), each one aligned to one of the low-quality P-frames. These warps are concatenated channel-wise with the low-quality P-frames to create a 6 channel input. This is projected to a 64-dimensional feature space and then processed using 10 residual blocks to yield the high-quality P-frame. This process is shown in the pink boxes of Figure 3.

## 4.2. Loss Functions

Restoring videos which were subject to extreme compression is a challenging problem. In general, we found that

traditional regression losses alone produce a blurry result. This is directly caused by lossy compression’s preference for removing high frequency details which is true for both images and videos. We use two loss functions during training in order to solve this problem.

**Regression Loss** We use the  $l_1$  error as our regression loss. For network output  $O$  and target frame  $T$  we compute

$$\mathcal{L}_1(O, T) = \|T - O\|_1 \quad (1)$$

**Scale-Space Loss** We use a loss based on the Difference of Gaussians (DoG) scale space [14]. The DoG is a fast approximation to the Laplacian of Gaussians and as such functions as a band-pass filter. By isolating these frequency bands and weighting their error equally, the network is encouraged to generate images which match in more than just the low-frequency regions. Formally, given network output  $O$  and target frame  $T$ , we compute 4 scales by downsampling  $O$ , yielding the scale space

$$S = \{O, O_2, O_4, O_8\} \quad (2)$$

where entry  $O_s$  is obtained by downsampling  $O$  by the factor  $s$  in both the width and height. We then compute the DoG by convolving each entry in  $S$  with  $5 \times 5$  2D gaussian kernels of increasing standard deviation  $\sigma$ :

$$G(\sigma)_{ij} = \frac{1}{2\pi\sigma^2} e^{-\frac{i^2+j^2}{2\sigma^2}} \quad (3)$$

for kernel offsets  $i, j$ . For each scale  $s$  we compute four filtered images

$$\begin{aligned} I_{O,s,1} &= G(1.1) * O_s \\ I_{O,s,2} &= G(2.2) * O_s \\ I_{O,s,3} &= G(3.3) * O_s \\ I_{O,s,4} &= G(4.4) * O_s \end{aligned} \quad (4)$$

where  $*$  is the discrete, valid cross-correlation operator. We then compute the difference

$$\begin{aligned} B_{O,s,1} &= I_{O,s,2} - I_{O,s,1} \\ B_{O,s,2} &= I_{O,s,3} - I_{O,s,2} \\ B_{O,s,3} &= I_{O,s,4} - I_{O,s,3} \end{aligned} \quad (5)$$

Table 2. **Throughput.** We measure throughput (FPS) on an *NVIDIA GTX 1080 Ti* GPU. Despite having nearly twice as many parameters our network is faster than or on-par with prior works.

Method	240p	480p	720p	1080p	Parameters (M)
MFQE 1.0	12.6	3.8	1.6	0.7	1.788
MFQE 2.0	25.3	8.4	3.7	1.7	0.255
STDF-R1	38.9	9.9	4.2	1.8	0.330
STDF-R3L	23.8	5.9	2.5	1.0	1.275
<b>MetaBit (Ours)</b>	26.9	5.4	2.2	1.0	2.449

to yield the per-scale frequency bands. This process is repeated for the target image yielding  $B_T$ . The final loss is then the sum of absolute error between the frequency bands

$$\mathcal{L}_{\text{DoG}}(O, T) = \sum_{s \in \{1, 2, 4, 8\}} \sum_{b=1}^3 \|B_{T,s,b} - B_{O,s,b}\|_1 \quad (6)$$

**GAN and Texture Losses** We use the Wassertein GAN formulation  $\mathcal{L}_W(O, T)$  [47] with a critic modeled after DC-GAN [48], which we modified using the procedure in Chu *et al.* [49] to introduce temporal consistency (Appendix B). We include a texture loss [26] which replaces the traditional ImageNet trained perceptual loss with a VGG [50] network trained on the MINC materials dataset [51]. Intuitively, if the images are encouraged to produce similar logits from this MINC-trained VGG, then it is likely the two images would be classified as the same material and therefore have similar textures. We compare feature maps from layer 5 convolution 3 of this VGG network. Formally:

$$\mathcal{L}_{\text{texture}}(O, T) = \|\text{MINC}_{5,3}(T) - \text{MINC}_{5,3}(O)\|_1 \quad (7)$$

**Composite Loss Function** This yields the following two loss functions, a regression loss

$$\mathcal{L}_R(O, T) = \alpha \mathcal{L}_1(O, T) + \beta \mathcal{L}_{\text{DoG}}(O, T) \quad (8)$$

which is used for regression-only experiments and GAN pretraining. And a GAN loss

$$\mathcal{L}_{\text{GAN}}(O, T) = \alpha \mathcal{L}_1(O, T) + \beta \mathcal{L}_{\text{DoG}}(O, T) + \gamma \mathcal{L}_W(O, T) + \delta \mathcal{L}_{\text{texture}}(O, T) \quad (9)$$

where  $\alpha, \beta, \gamma, \delta$  are balancing hyperparameters.

## 5. Experiments and Results

The final architecture as described in Section 4 contains nearly twice the parameters of the previous state-of-the-art without performing any motion estimation or detection of high quality frames and restores 7 frame blocks. We now show empirically that this formulation surpasses prior works on historical compression correction benchmarks as well as more realistic compression settings, often by a large margin. Our method does this while maintaining roughly the same throughput as the previous best method.

Table 3. **GAN Scores.** The GAN loss allows our network to generate more realistic images than the regression loss alone. Regression loss leads to worse FID scores caused by the smooth, textureless appearance of scene elements. Format is FID ↓ / LPIPS ↓

Method	H.264 CRF	
	40	50
H.264 (Degraded Input)	67.07 / 0.259	152.19 / 0.498
MetaBit (Regression)	80.67 / 0.265	154.42 / 0.482
<b>MetaBit (GAN)</b>	<b>37.78 / 0.191</b>	<b>95.26 / 0.368</b>

### 5.1. Datasets

We train on the MFQE dataset [11] training split (108 variable length sequences) augmented with a randomly selected one-third of the Vimeo90k dataset [29] training split (approximately 30,000 7-frame sequences). We randomly crop  $256 \times 256$  patches from each example and apply random horizontal and vertical flipping. For H.264 benchmarks, we encode the resulting sequence with a 7 frame GOP and no B-frames, thus yielding one I-frame and 6 P-frames per example. We use CRF encoding for H.264 benchmarks. For H.265 benchmarks, to comply with prior works, we use CQP encoding with the same 7-frame GOP and no B-frames. Please see Appendix C for the exact compression commands we used. We evaluate on the MFQE test split. This consists of 18 variable-length sequences (7890 frames) commonly used for evaluation of compression algorithms and was proposed by the Joint Collaborative Team on Video Coding [52].

### 5.2. Training Procedure

Our network is implemented using PyTorch [53] and trained end-to-end for 200 epochs using the Adam optimizer [54] with a learning rate of  $10^{-4}$ . We do not lower this learning rate during training. For quantitative benchmarks, we train using the regression loss (Equation 8) with  $\alpha = 1.0, \beta = 1.0$ .

For GAN training, we begin with regression weights and fine-tune the entire network using our GAN loss (Equation 9) with  $\alpha = 0.01, \beta = 0.01, \gamma = 0.005, \delta = 1$ . We train for an additional 200 epochs with a learning rate of  $10^{-5}$  and the RMSProp optimizer.

For regression we report the change in PSNR and change in LPIPS [55] averaged over all frames in the test set. LPIPS is only computed for models we were able to retrain for our evaluation. To ensure a fair comparison with prior works, we compute metrics only on the Y channel of YCbCr images where the color transform is defined by the ITU-R BT.601 standard. For GAN evaluation, we report the average FID score [56] of the compressed and restored frames. This metric is widely used as a measure of the “realism” of an image in lieu of a user study.



Figure 5. **Qualitative Results.** Please zoom in to view fine details. Note the increased quality of the MetaBit model over STDF and the enhanced sharpness and textures of the GAN method. This is particularly apparent on the trees (row 1), car (row 2), grass (row 3), and the wood texture (row 4). Additional qualitative results are shown in Appendix F and the attached supplement.

**SSIM Metric** We found no conclusive trend in SSIM [57] results (reported in Appendix D). Despite large changes in PSNR and LPIPS, SSIM results seem to change little if at all, particularly when compared to the gains reported in JPEG correction literature (Jiang *et al.* [28] for example). This is likely caused by the in-loop deblocking filter present in modern codecs and is discussed further in Appendix D.

### 5.3. Comparison to the State-of-the-Art

Our method achieves state-of-the-art results both on the H.265 benchmarks proposed in prior works and in the much more widely applicable H.264 benchmarks we propose here. We compare to MFQE 1.0 [11], MFQE 2.0 [13], and STDF [12]. We do not compare with single-frame video restoration methods or image restoration methods which were found to have objectively worse performance than the multiframe methods. Table 1 shows our state-of-the-art results. We compare H.265 with constant QPs in {27, 32, 37} and use publication-reported numbers. For H.264, we retrain prior works using published code and procedures and test on CRF values in {25, 35, 40, 50}. Note that MFQE 1.0 has no published code and MFQE 2.0 failed to converge for any CRF training. We test STDF in both the R1 (3-frame sliding window) and the R3 (7-frame sliding window) setting.

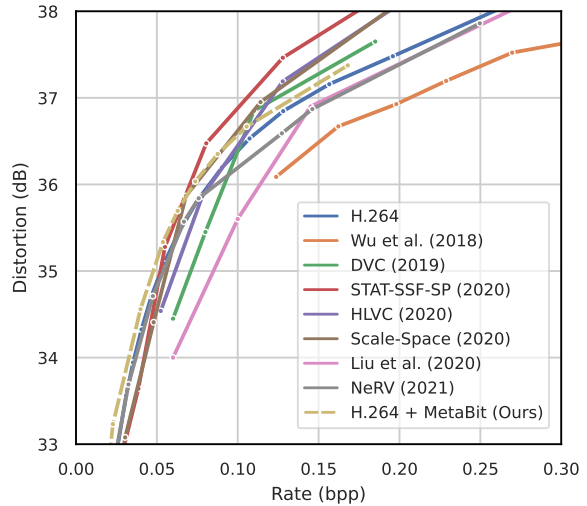


Figure 6. **UVG Rate-Distortion.** Distortion is measured with PSNR. Using H.264 + MetaBit method surpasses recent fully deep-learning codecs at low bitrates. As expected, the improvement reduces as bitrate increases.

Overall our method makes an advancement in PSNR and LPIPS improvement over prior works. In particular, we note that in prior works as compression decreases (lower CQP or CRF settings) performance is also decreased. Conversely,



Table 4. **Compression Throughput.** We measure FPS on an *NVIDIA GTX 2080 Ti* GPU compared to recent deep-learning-based codecs on 1080p frames. For encoding, our method uses H.264 and there is no GPU requirement. NeRV [58] encoding speed is not directly reported but requires training a unique network per video.

	Wu <i>et al.</i> [59]	DVC [60]	Liu <i>et al.</i> [61]	NeRV [58]	MetaBit (Ours)
Decoding $10^{-3}$	1.8	3		<b>12.5</b>	<u>3.42</u>
Encoding 2.4	1.5	2		-	<b>52</b>

our formulation is able to better leverage information from the higher quality I-Frames yielding larger improvements.

We also provide throughput results in Table 2. Note that despite having more parameters and better restoration results, our method achieves similar throughput to STDF, the prior state-of-the-art, even exceeding it in some cases. Our method is also comparable in speed to MFQE 2.0 which has 9 times fewer parameters. Note that these tests were performed in like-conditions to those reported by prior works to control for the compute environment.

#### 5.4. Extreme Compression

While the quantitative results on CRF values  $\{40, 50\}$  show an improvement in PSNR, these settings represent extreme compression. We found that the regression result of our network is not visually pleasing despite the improvement, so we additionally show results using our GAN procedure. Quantitatively, FID scores in Table 3 show a significant improvement in realism with LPIPS scores similarly indicating a significant improvement in perceptual similarity. We show qualitative results in Figure 5, note the significantly improved textures, sharp edges, and additional detail introduced by the GAN loss, particularly compared to STDF.

#### 5.5. Comparison to Learned Video Compression

One application for this work is as a stopgap technology between classical compression and fully deep-learning-based compression. This allows for the speed, memory consumption, and technical debt associated with classical compression algorithms to sustain, with bitstreams fully decodable by users who lack the computational resources for deep models. In Table 4, we compare the frame-rate of our method against recently published learned video compression algorithms, and in Figure 6, we compare rate-distortion on the UVG [62] dataset. Our method is only bested by the recent NeRV [58] for throughput (which we note has extremely long encoding times) and achieves better rate-distortion results than many compared methods especially at low bitrates.

#### 5.6. Ablation

We ablate our design in Table 5, showing impact on throughput and reconstruction accuracy. Note that the first row in each section is the “reference” method, *i.e.*, the final model tested in previous sections.

Table 5. **Ablation.** Inference FPS is computed on an *NVIDIA GTX 1080 Ti* for 240p frames, PSNR is computed for H.264 CRF 25.

Property	Option	Result	
		$\Delta$ PSNR (dB)	FPS
Parameter Distribution	Favors I-Frames	<b>0.954</b>	<b>26.9</b>
	Even	0.938 (-1.6%)	24.3 (-9.7%)
Motion Compensation	Motion Vectors	0.948	26.9
	Optical Flow	<b>0.952 (+0.4%)</b>	17.0 (-36.8%)
	None	0.938 (-1.1%)	<b>27.6 (+2.6%)</b>
Loss	$l_1$ and Scale-Space	<b>0.954</b>	-
	$l_1$ Only	0.900 (-5.6%)	-

**Parameter Distribution** Our architecture allocates more parameters to the I-frame representation than the P-frame representation (64- vs. 16- dimensional). Here, we compare with an “even” distribution that allocates a 32-dimensional representation to both. This performs worse in all regards.

**Motion Compensation** We use video motion vectors to perform feature alignment. A natural comparison is between using per-pixel optical flow or doing no alignment at all. For optical flow, we use a pre-trained RAFT [16] model and find that indeed the fine motion detail does improve performance but at a significant throughput penalty, while performing no alignment decreases performance.

**Loss** We claimed in Section 4.2 that our scale-space loss helps ensure a correct reconstruction of higher frequency information leading to better reconstruction accuracy. We test this and find that it indeed leads to a 5.6% improvement over not using a scale-space loss.

### 6. Conclusion and Future Work

We presented a novel formulation for video compression correction. Our network leverages the structure of the compressed bitstream to outperform prior works on standard benchmarks, as well as newly proposed settings with wider applicability, while still being extremely efficient. This work has the potential to help people (see the ethics discussion in Appendix A) in bandwidth-constrained environments by allowing heavily compressed bitstreams to be viewable.

While our work is an important step towards practical adoption of these techniques, we hope that it will inspire additional research. Particularly: high-resolution video is slow to process and time-varying compression artifacts can introduce temporal inconsistencies (see video examples in the attached supplement). Further research is required to make such restoration practical. Nevertheless, given our favorable comparison to fully deep-learning methods, we believe that this technology is an important stopgap between classical compression and fully deep-learning compression. Importantly, this technology will be usable in the near-term and will be able to reach a wider audience sooner than fully deep-learning based codecs. Therefore, the community would benefit from increased investigation into this technology.

## References

- [1] A. Oentoro, *Video marketing statistics and strategy 2021*, Oct. 2021. [Online]. Available: <https://breadnbeyond.com/video-marketing/video-marketing-strategies-statistics/>.
- [2] M. Duggan, *Photo and video sharing grow online*, May 2020. [Online]. Available: <https://www.pewresearch.org/internet/2013/10/28/photo-and-video-sharing-grow-online/>.
- [3] D. Marpe, T. Wiegand, and G. J. Sullivan, "The h.264/mpeg4 advanced video coding standard and its applications," *IEEE communications magazine*, vol. 44, no. 8, pp. 134–143, 2006.
- [4] D. Mukherjee, J. Han, J. Bankoski, R. Bultje, A. Grange, J. Koleszar, P. Wilkins, and Y. Xu, "A technical overview of vp9—the latest open-source video codec," *SMPTE Motion Imaging Journal*, vol. 124, no. 1, pp. 44–54, 2015.
- [5] G. J. Sullivan, J.-R. Ohm, W.-J. Han, and T. Wiegand, "Overview of the high efficiency video coding (hevc) standard," *IEEE Transactions on circuits and systems for video technology*, vol. 22, no. 12, pp. 1649–1668, 2012.
- [6] Y. Chen, D. Murherjee, J. Han, A. Grange, Y. Xu, Z. Liu, S. Parker, C. Chen, H. Su, U. Joshi, *et al.*, "An overview of core coding tools in the av1 video codec," in *2018 Picture Coding Symposium (PCS)*, IEEE, 2018, pp. 41–45.
- [7] J. Bankoski, P. Wilkins, and Y. Xu, "Technical overview of vp8, an open source video codec for the web," in *2011 IEEE International Conference on Multimedia and Expo*, IEEE, 2011, pp. 1–6.
- [8] B. Auxier and M. Anderson, *Social media use in 2021*, Apr. 2021. [Online]. Available: <https://www.pewresearch.org/internet/2021/04/07/social-media-use-in-2021/>.
- [9] Y. LeCun, B. E. Boser, J. S. Denker, D. Henderson, R. E. Howard, W. E. Hubbard, and L. D. Jackel, "Handwritten digit recognition with a back-propagation network," in *Advances in neural information processing systems*, 1990, pp. 396–404.
- [10] I. Sutskever, G. E. Hinton, and A. Krizhevsky, "Imagenet classification with deep convolutional neural networks," *Advances in neural information processing systems*, pp. 1097–1105, 2012.
- [11] R. Yang, M. Xu, Z. Wang, and T. Li, "Multi-frame quality enhancement for compressed video," in *2018 IEEE/CVF Conference on Computer Vision and Pattern Recognition*, IEEE, Jun. 2018, pp. 6664–6673, ISBN: 978-1-5386-6420-9. DOI: [10.1109/CVPR.2018.00697](https://doi.org/10.1109/CVPR.2018.00697). [Online]. Available: <https://ieeexplore.ieee.org/document/8578795/>.
- [12] J. Deng, L. Wang, S. Pu, and C. Zhuo, "Spatio-temporal deformable convolution for compressed video quality enhancement," *Proceedings of the AAAI Conference on Artificial Intelligence*, vol. 34, no. 0707, pp. 10 696–10 703, Apr. 2020, ISSN: 2374-3468. DOI: [10.1609/aaai.v34i07.6697](https://doi.org/10.1609/aaai.v34i07.6697).
- [13] Q. Xing, Z. Guan, M. Xu, R. Yang, T. Liu, and Z. Wang, "Mfqc 2.0: A new approach for multi-frame quality enhancement on compressed video," *IEEE Transactions on Pattern Analysis and Machine Intelligence*, vol. 43, no. 3, pp. 949–963, Mar. 2021, arXiv: 1902.09707, ISSN: 0162-8828, 2160-9292, 1939-3539. DOI: [10.1109/TPAMI.2019.2944806](https://doi.org/10.1109/TPAMI.2019.2944806).
- [14] D. G. Lowe, "Object recognition from local scale-invariant features," in *Proceedings of the seventh IEEE international conference on computer vision*, Ieee, vol. 2, 1999, pp. 1150–1157.
- [15] I. Goodfellow, J. Pouget-Abadie, M. Mirza, B. Xu, D. Warde-Farley, S. Ozair, A. Courville, and Y. Bengio, "Generative adversarial nets," *Advances in neural information processing systems*, vol. 27, 2014.
- [16] Z. Teed and J. Deng, "Raft: Recurrent all-pairs field transforms for optical flow," in *European conference on computer vision*, Springer, 2020, pp. 402–419.
- [17] G. K. Wallace, "The jpeg still picture compression standard," *IEEE transactions on consumer electronics*, vol. 38, no. 1, pp. xviii–xxxiv, 1992.
- [18] C. Dong, Y. Deng, C. Change Loy, and X. Tang, "Compression artifacts reduction by a deep convolutional network," in *Proceedings of the IEEE International Conference on Computer Vision*, 2015, pp. 576–584.
- [19] P. Svoboda, M. Hradis, D. Barina, and P. Zemcik, "Compression artifacts removal using convolutional neural networks," *arXiv preprint arXiv:1605.00366*, 2016.
- [20] L. Cavigelli, P. Hager, and L. Benini, "Cas-cnn: A deep convolutional neural network for image compression artifact suppression," in *2017 International Joint Conference on Neural Networks (IJCNN)*, IEEE, 2017, pp. 752–759.

- [21] X. Liu, X. Wu, J. Zhou, and D. Zhao, "Data-driven sparsity-based restoration of jpeg-compressed images in dual transform-pixel domain," in *Proceedings of the IEEE Conference on Computer Vision and Pattern Recognition*, 2015, pp. 5171–5178.
- [22] X. Zhang, W. Yang, Y. Hu, and J. Liu, "Dmcnn: Dual-domain multi-scale convolutional neural network for compression artifacts removal," in *2018 25th IEEE International Conference on Image Processing (ICIP)*, IEEE, 2018, pp. 390–394.
- [23] B. Zheng, Y. Chen, X. Tian, F. Zhou, and X. Liu, "Implicit dual-domain convolutional network for robust color image compression artifact reduction," *IEEE Transactions on Circuits and Systems for Video Technology*, 2019.
- [24] Z. Wang, D. Liu, S. Chang, Q. Ling, Y. Yang, and T. S. Huang, "D3: Deep dual-domain based fast restoration of jpeg-compressed images," in *Proceedings of the IEEE Conference on Computer Vision and Pattern Recognition*, 2016, pp. 2764–2772.
- [25] P. Liu, H. Zhang, K. Zhang, L. Lin, and W. Zuo, "Multi-level wavelet-cnn for image restoration," in *Proceedings of the IEEE Conference on Computer Vision and Pattern Recognition Workshops*, 2018, pp. 773–782.
- [26] M. Ehrlich, L. Davis, S.-N. Lim, and A. Shrivastava, "Quantization guided jpeg artifact correction," *Proceedings of the European Conference on Computer Vision*, 2020.
- [27] —, "Analyzing and mitigating jpeg compression defects in deep learning," in *Proceedings of the IEEE/CVF International Conference on Computer Vision*, 2021, pp. 2357–2367.
- [28] J. Jiang, K. Zhang, and R. Timofte, "Towards flexible blind jpeg artifacts removal," in *Proceedings of the IEEE/CVF International Conference on Computer Vision*, 2021, pp. 4997–5006.
- [29] T. Xue, B. Chen, J. Wu, D. Wei, and W. T. Freeman, "Video enhancement with task-oriented flow," *International Journal of Computer Vision*, vol. 127, no. 8, pp. 1106–1125, Aug. 2019, arXiv: 1711.09078, ISSN: 0920-5691, 1573-1405. DOI: [10.1007/s11263-018-01144-2](https://doi.org/10.1007/s11263-018-01144-2).
- [30] X. Wang, K. C. Chan, K. Yu, C. Dong, and C. Change Loy, "Edvr: Video restoration with enhanced deformable convolutional networks," in *Proceedings of the IEEE/CVF Conference on Computer Vision and Pattern Recognition Workshops*, 2019, pp. 0–0.
- [31] J. Dai, H. Qi, Y. Xiong, Y. Li, G. Zhang, H. Hu, and Y. Wei, "Deformable convolutional networks," in *Proceedings of the IEEE international conference on computer vision*, 2017, pp. 764–773.
- [32] Y. Jo, S. W. Oh, J. Kang, and S. J. Kim, "Deep video super-resolution network using dynamic upsampling filters without explicit motion compensation," in *Proceedings of the IEEE conference on computer vision and pattern recognition*, 2018, pp. 3224–3232.
- [33] K. C. Chan, X. Wang, K. Yu, C. Dong, and C. C. Loy, "Basicvsr: The search for essential components in video super-resolution and beyond," in *Proceedings of the IEEE/CVF Conference on Computer Vision and Pattern Recognition*, 2021, pp. 4947–4956.
- [34] Y. Li, P. Jin, F. Yang, C. Liu, M.-H. Yang, and P. Milanfar, "Comisr: Compression-informed video super-resolution," in *Proceedings of the IEEE/CVF International Conference on Computer Vision (ICCV)*, Oct. 2021, pp. 2543–2552.
- [35] T. Wang, M. Chen, and H. Chao, "A novel deep learning-based method of improving coding efficiency from the decoder-end for hevc," in *2017 Data Compression Conference (DCC)*, IEEE, 2017, pp. 410–419.
- [36] R. Yang, M. Xu, T. Liu, Z. Wang, and Z. Guan, "Enhancing quality for hevc compressed videos," *IEEE Transactions on Circuits and Systems for Video Technology*, vol. 29, no. 7, pp. 2039–2054, 2018.
- [37] C. Cortes and V. Vapnik, "Support-vector networks," *Machine learning*, vol. 20, no. 3, pp. 273–297, 1995.
- [38] M. Schuster and K. K. Paliwal, "Bidirectional recurrent neural networks," *IEEE transactions on Signal Processing*, vol. 45, no. 11, pp. 2673–2681, 1997.
- [39] Q. Ding, L. Shen, L. Yu, H. Yang, and M. Xu, "Patch-wise spatial-temporal quality enhancement for hevc compressed video," *IEEE Transactions on Image Processing*, vol. 30, pp. 6459–6472, 2021.
- [40] M. Zhao, Y. Xu, and S. Zhou, "Recursive fusion and deformable spatiotemporal attention for video compression artifact reduction," in *Proceedings of the 29th ACM International Conference on Multimedia*, 2021, pp. 5646–5654.
- [41] S. Tomar, "Converting video formats with ffmpeg," *Linux Journal*, vol. 2006, no. 146, p. 10, 2006.
- [42] K. He, X. Zhang, S. Ren, and J. Sun, "Deep residual learning for image recognition," in *Proceedings of the IEEE conference on computer vision and pattern recognition*, 2016, pp. 770–778.



- [43] S. Ioffe and C. Szegedy, “Batch normalization: Accelerating deep network training by reducing internal covariate shift,” in *International conference on machine learning*, PMLR, 2015, pp. 448–456.
- [44] X. Wang, K. Yu, S. Wu, J. Gu, Y. Liu, C. Dong, Y. Qiao, and C. Change Loy, “Esrgan: Enhanced super-resolution generative adversarial networks,” in *Proceedings of the European conference on computer vision (ECCV) workshops*, 2018, pp. 0–0.
- [45] Q. Wang, B. Wu, P. Zhu, P. Li, W. Zuo, and Q. Hu, “Eca-net: Efficient channel attention for deep convolutional neural networks, 2020 ieee,” in *CVF Conference on Computer Vision and Pattern Recognition (CVPR)*. IEEE, 2020.
- [46] A. Vaswani, N. Shazeer, N. Parmar, J. Uszkoreit, L. Jones, A. N. Gomez, Ł. Kaiser, and I. Polosukhin, “Attention is all you need,” in *Advances in neural information processing systems*, 2017, pp. 5998–6008.
- [47] M. Arjovsky, S. Chintala, and L. Bottou, “Wasserstein generative adversarial networks,” in *International conference on machine learning*, PMLR, 2017, pp. 214–223.
- [48] A. Radford, L. Metz, and S. Chintala, “Unsupervised representation learning with deep convolutional generative adversarial networks,” *arXiv preprint arXiv:1511.06434*, 2015.
- [49] M. Chu, Y. Xie, J. Mayer, L. Leal-Taixé, and N. Thuerrey, “Learning temporal coherence via self-supervision for gan-based video generation,” *ACM Transactions on Graphics (TOG)*, vol. 39, no. 4, pp. 75–1, 2020.
- [50] K. Simonyan and A. Zisserman, “Very deep convolutional networks for large-scale image recognition,” *arXiv preprint arXiv:1409.1556*, 2014.
- [51] S. Bell, P. Upchurch, N. Snaveley, and K. Bala, “Material recognition in the wild with the materials in context database,” in *Proceedings of the IEEE conference on computer vision and pattern recognition*, 2015, pp. 3479–3487.
- [52] J.-R. Ohm, G. J. Sullivan, H. Schwarz, T. K. Tan, and T. Wiegand, “Comparison of the coding efficiency of video coding standards—including high efficiency video coding (hevc),” *IEEE Transactions on circuits and systems for video technology*, vol. 22, no. 12, pp. 1669–1684, 2012.
- [53] A. Paszke, S. Gross, F. Massa, A. Lerer, J. Bradbury, G. Chanan, T. Killeen, Z. Lin, N. Gimelshein, L. Antiga, *et al.*, “Pytorch: An imperative style, high-performance deep learning library,” *Advances in neural information processing systems*, vol. 32, pp. 8026–8037, 2019.
- [54] D. P. Kingma and J. Ba, “Adam: A method for stochastic optimization,” *arXiv preprint arXiv:1412.6980*, 2014.
- [55] R. Zhang, P. Isola, A. A. Efros, E. Shechtman, and O. Wang, “The unreasonable effectiveness of deep features as a perceptual metric,” in *Proceedings of the IEEE conference on computer vision and pattern recognition*, 2018, pp. 586–595.
- [56] M. Heusel, H. Ramsauer, T. Unterthiner, B. Nessler, and S. Hochreiter, “Gans trained by a two time-scale update rule converge to a local nash equilibrium,” *Advances in neural information processing systems*, vol. 30, 2017.
- [57] Z. Wang, A. C. Bovik, H. R. Sheikh, and E. P. Simoncelli, “Image quality assessment: From error visibility to structural similarity,” *IEEE transactions on image processing*, vol. 13, no. 4, pp. 600–612, 2004.
- [58] H. Chen, B. He, H. Wang, Y. Ren, S.-N. Lim, and A. Shrivastava, “Nerv: Neural representations for videos,” *arXiv preprint arXiv:2110.13903*, 2021.
- [59] C.-Y. Wu, N. Singhal, and P. Krahenbuhl, “Video compression through image interpolation,” in *Proceedings of the European Conference on Computer Vision (ECCV)*, 2018, pp. 416–431.
- [60] G. Lu, W. Ouyang, D. Xu, X. Zhang, C. Cai, and Z. Gao, “Dvc: An end-to-end deep video compression framework,” in *Proceedings of the IEEE/CVF Conference on Computer Vision and Pattern Recognition*, 2019, pp. 11 006–11 015.
- [61] J. Liu, S. Wang, W.-C. Ma, M. Shah, R. Hu, P. Dhawan, and R. Urtasun, “Conditional entropy coding for efficient video compression,” in *Computer Vision—ECCV 2020: 16th European Conference, Glasgow, UK, August 23–28, 2020, Proceedings, Part XVII 16*, Springer, 2020, pp. 453–468.
- [62] A. Mercat, M. Viitanen, and J. Vanne, “Uvg dataset: 50/120fps 4k sequences for video codec analysis and development,” in *Proceedings of the 11th ACM Multimedia Systems Conference*, 2020, pp. 297–302.

## A. Statement of Ethical Impact

After careful consideration, we find no specific ethical concerns with the work presented in this paper. To the contrary, we believe that improved compression algorithms are a way to make the internet more inclusive and sustainable. Our work fits into the larger context of compression research, and is a way to make existing compression algorithms function better (*i.e.*, by improving their rate-distortion performance). Many communities across the world do not have access to reliable internet, and although this is changing in certain areas, it has stagnated in others. Improving the reliability of internet infrastructure is time consuming and costly, however, making transmissions more efficient is a software concern that can effectively mitigate some of the issues caused by unreliable internet. *Our method makes video transmissions more efficient* and we believe that techniques such as ours can be made computationally efficient enough to be useful in the near-term. Especially in a time when video communication is increasingly necessary for work and school, we believe that this work can genuinely help those in need.

## B. GAN Architecture Details

Chu *et al.* [49] introduce a temporally consistent formulation for video GAN discriminators. We adapt their idea in our GAN loss which is otherwise based on DCGAN [48]. The architecture is shown in Figure 7.

Our critic operates on triplets of the compressed frames  $C$ , network outputs  $O$ , and target frames  $T$ . The input frames are stacked channelwise, in other words  $C_{0,R}, C_{0,G}, C_{0,B}, \dots, C_{6,R}, C_{6,G}, C_{6,B}$  for all frames in the GOP are stacked channel-wise along with the corresponding  $O$  or  $T$  frames to create a 48 channel input (3 channels per frame, times 7 frames, times 2). The task for the critic, then, is to determine whether the  $T$  or  $O$  channels are network outputs or uncompressed frames given the compressed reference frames and otherwise operates as standard DCGAN. The output is used in a Wasserstein GAN loss [47].

This encourages temporal consistency because the critic is judging the entire 7-frame sequence as an example as opposed to other video GANs which treat each frame as an different example. In the later case, there may be situations in which one frame is judged to be more real than another, and yet all frames are equally “real” or “fake”. This “reallness” or “fakeness” of the sequence *vs.* the frames is better captured by the formulation of Chu *et al.* [49]. Note that for our task we define “fake” as the restored network output and “real” as the uncompressed version of the image.

## C. Compression Details

The MFQE [11] dataset is stored as a series of uncompressed raw (.yuv) videos of known resolution and frame count. We compress these videos using ffmpeg [41]. For

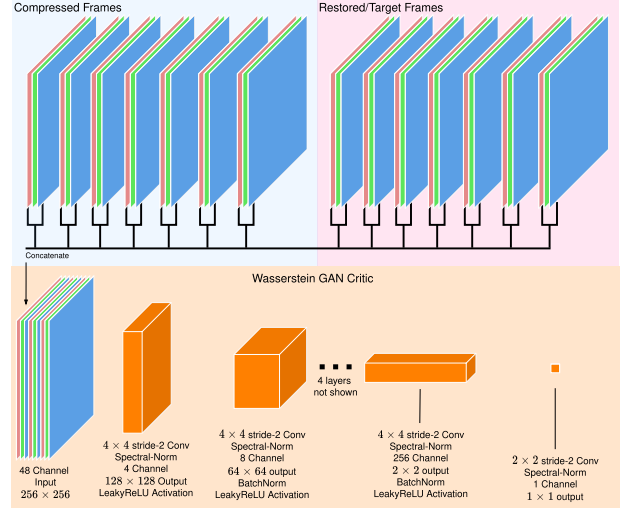


Figure 7. **Wasserstein GAN Critic.** Inputs (top) are RGB channels for all 7 frames stacked in the channel dimension. The compressed frames are concatenated with the restored or target frames for a 48 channel input. This is then processed by 8 downsampling convolutional layers as in DCGAN to produce the critic output.

H.264, we use the libx264 encoder with the following command:

```
ffmpeg ffmpeg -video_size <WIDTH>x<HEIGHT> \
  -framerate 10 \
  -i <INPUT> \
  -preset medium \
  -vcodec libx264 \
  -crf <CRF> \
  -x264opts <OPTIONS> \
  [OUTPUT]
```

where <OPTIONS> is defined as:

```
keyint=7:min-keyint=7:no-scenecut:
no-fast-pskip:me=esa:subme=7:bframes=0
```

This produces a compressed .mp4 file for later use (to be read as-is or converted back to raw .yuv for compatibility with prior work). Many of these options are simply there to ensure a 7 frame GOP which is a requirement of the model we presented in the body of the paper (but **not** a requirement of the general method which we presented). Please note the `-framerate 10` argument: CRF is sensitive to framerate, so different framerates will incur different degradation strengths. Our choice of 10 was arbitrary and motivated primarily by recommendation of Li *et al.* [34].

For H.264 in “streaming mode” (Appendix E) we use the following command in order to be consistent with deep-learning-based compression works:



Figure 8. **Codec Comparison.** HM reference encoder vs. libx265 at QP37. While the artifacts produced by the different encoders are different, the overall perceptual quality is similar. This is likely because of CQP encoding which does not leave many options for the encoder to make intelligent rate-distortion decisions.

```
ffmpeg -video_size <WIDTH>x<HEIGHT> \
  -framerate 30 \
  -i <INPUT> \
  -crf <CRF> \
  -preset medium \
  -vcodec libx264 \
  -pix_fmt yuv420p \
  -x264opts keyint_min=10000:bframes=0 \
  <OUTPUT>
```

Here, `keyint_min=10000` ensures that there is only a single I-frame per video.

For H.265, prior works evaluated on the HM reference codec, which is notoriously slow. For any models which we retrained on H.265 data, we instead use libx265 which incurs no appreciable change in degradation (Figure 8) and is significantly faster than HM. To generate these videos we used the following command:

```
ffmpeg -video_size <WIDTH>x<HEIGHT> \
  -i <INPUT> \
  -vcodec libx265 \
  -qp <QP> \
  -x265-params <OPTIONS> \
  <OUTPUT>
```

for <OPTIONS>:

```
keyint=7:min-keyint=7:no-scenecut:
me=full:subme=7:bframes=0:qp=<QP>
```

Note that QP is specified twice and there is no longer a need to control for framerate. We strongly recommend that future works use libx265.

Table 6. **SSIM Comparison.** Format is  $\Delta$ PSNR /  $\Delta$  SSIM. Best PSNR shown in **Bold**, best SSIM shown in Underline.

Method	H.264 CRF			
	25	35	40	50
STDF-R1 [12]	0.741 / 0.006	0.862 / 0.011	0.814 / 0.015	0.632 / 0.023
STDF-R3 [12]	0.784 / 0.006	0.846 / 0.010	0.882 / 0.015	0.817 / 0.027
<b>MetaBit (Ours)</b>	<b>1.085</b> / 0.002	<b>1.137</b> / 0.013	<b>1.130</b> / 0.015	<b>0.887</b> / 0.012

Table 7. **Deblocking Filter Comparison.**

	Deblocking Filter	No Deblocking Filter
Compressed (H.264 CRF 40)	0.79731	0.78445
Restored (Ours)	0.81261 (+0.0153/+1.92%)	0.81523 (+0.03078/+3.92%)
Compressed (JPEG Quality 7)	-	0.78435
Restored (QGAC [26])	-	0.84848 (+0.06413/+8.18%)

## D. SSIM And Metrics

During evaluation we found no usable trend in SSIM metrics. Often large and appreciable changes in PSNR and LPIPS were not matched by changes in SSIM. In Table 6 we reproduce the H.264 PSNR results presented in the body of the paper with the addition of SSIM metrics compared to the two STDF [12] models. Note that for CRF 25, STDF-R1 makes an objective improvement over STDF-R3 in PSNR, yet the SSIM delta is unchanged. Moreover, note that our model has significantly better performance in terms of both PSNR and yet has decreased SSIM performance. While our model is not inferior on SSIM for all metrics, this behavior is odd.

We can explain this behavior by examining the in-loop deblocking filter that is included in modern MPEG codecs (both H.264 and H.265 use a deblocking filter). This deblocking filter is a heuristic, non-linear, non-differentiable transform applied to the frames by the decoder along mac-





Figure 9. **Qualitative Deblocking Comparison.** First row: degraded, second row: restored. H.264 frames were corrected with our model, the JPEG frame was corrected with QGAC [26]. The H.264 deblocking filter improves image quality and skews SSIM results. Disabling the filter results in a larger SSIM delta but not necessarily a larger overall SSIM. The JPEG image, despite appearing significantly more degraded than the H.264 without filtering, has almost the same SSIM.

roblock boundaries and has the effect of reducing the overall variance of the block. For brevity, we do not define the in-loop filter here but it can be found in the relevant standards documents. Recall that SSIM [44] is (commonly) defined on  $11 \times 11$  windows  $x, y$  as

$$\text{SSIM}(x, y) = \frac{(2\mu_x\mu_y + c_1)(2\sigma_{xy} + c_2)}{(\mu_x^2\mu_y^2 + c_1)(\sigma_x^2\sigma_y^2 + c_2)} \quad (10)$$

Since SSIM is defined in terms of the means ( $\mu$ ) and variances ( $\sigma^2$ ) of the two windows, and the MPEG deblocking filter explicitly reduces these values, we attribute the lack of SSIM trend to this deblocking filter.

This can be shown empirically in several ways. Firstly, we simply disable the deblocking filter and observing the change in SSIM value (Table 7). Next, we can compare with JPEG artifact correction literature. For each frame, we use JPEG to compress to roughly the same SSIM (Figure 9) and compute the difference in SSIM using *vs.* QGAC [26] restoration on the JPEG compressed frame. Table 7 also shows the SSIM performance comparison for our method *vs.* JPEG. These empirical results show that simply disabling the deblocking filter allows video correction models to improve SSIM to a much greater degree and, at least at the dataset level, improve SSIM further than starting with the deblocking-filtered frame.

However, doing this would be solely for the benefit of producing an otherwise fairly meaningless quantitative result. Notice in Figure 9 that the JPEG image appears to be of much worse quality despite having similar SSIM to the H.264 frames, so its usefulness as a perceptual similarity metric is limited. Instead, we argue that future works should simply

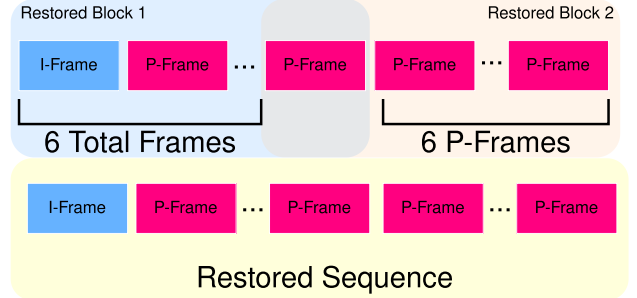


Figure 10. **Streaming Mode.** In streaming mode, the last restored P-frame in each block is cached and used instead of an I-frame for the next block.

report PSNR as a measure of “pure error” and LPIPS [55] as a measure of perceptual similarity.

## E. Streaming Mode

In many streaming applications, only a single I-frame is ever transmitted, with every subsequent frame stored as a P-frame. This saves bandwidth and decreases latency at the expense of quality. The model as described in the body of the paper requires a 7-frame GOP with a single I-frame followed by 6 P-frames, however, our model can be easily modified to operate in what we call “streaming mode”.

In streaming mode (Figure 10), our method performs a 7-frame restoration as usual on the first 7 frames which include the I-frame. The last restored P-frame (frame 7) is cached and used in place of the I-frame for the next 6 P-frames. This

process is repeated for all subsequent groups of 6 P-frames, eliminating the need for a periodic high-information frame. This comes at a small cost to restoration performance however it also greatly reduces the bitrate of the H.264 videos. This mode was used to produce the rate-distortion comparisons to deep-learning based compression which requires aggressive settings to match the bitrates reported in the compared works. Adding periodic I-frame incurs a large increase in bitrate.

## F. Additional Qualitative Results

In this section we show additional qualitative results. These results are intended to showcase particular strengths and weaknesses we observed in our model, and are explained further in the figure captions. We encourage viewing the video files contained in our supplementary material to observe temporal consistency issues we noticed due to fluctuating compression artifacts.

1. **Dark Region** Figure 11 highlights a known failure mode of compression causing additional information loss in dark areas in an image.
2. **Crowd** Figure 12 shows our model performance on a dense crowd
3. **Texture Restoration** Figure 13 shows an additional result of our model generating a plausible reconstruction of an artificial texture
4. **Compression Artifacts** Figure 14; one particular failure mode we observed was compression artifacts, particularly chroma subsampling artifacts, mistaken as a degraded texture and restored by the GAN, creating texture where none exists in the original images
5. **Motion Blur** Figure 15. Another common occurrence is missing motion blur in reconstructed images. There are several issues that lead to this: 1) high motion frames are largely absent from the training data, 2) motion blur is largely destroyed by compression, and 3) the reconstruction loss is explicitly rewarded for generating sharp restorations, whereas in this case we actually *want* a blurry reconstruction.
6. **Artificial** Figure 16; in this scene from the short film “Big Buck Bunny”, the frame is restored quite accurately despite a lack of artificial training data.

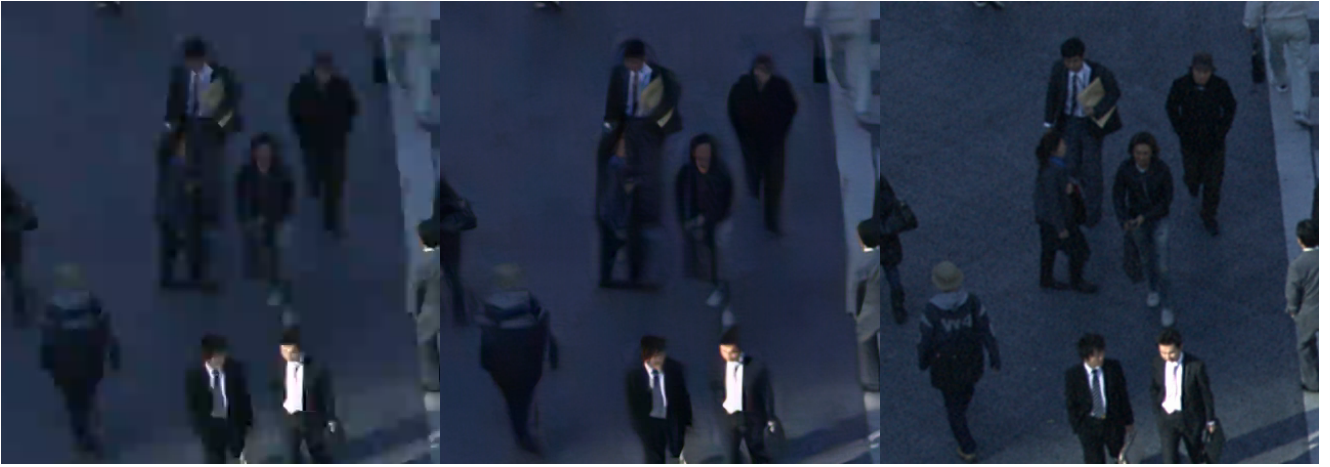


Figure 11. **Dark Region.** Crop from  $2560 \times 1600$  “People on Street”. The dark region, is poorly preserved by compression. Our GAN restoration struggles to cope with the massive information loss in this region.



Figure 12. **Crowd.** Crop from  $2560 \times 1600$  “People on Street”. The image shows an extremely dense crowd. Despite the chaotic nature, our GAN is able to produce a good restoration although there is detail missing.



Figure 13. **Texture Restoration.** Crop from  $1920 \times 1080$  “Cactus”. The texture on the background is destroyed by compression. Our GAN reconstructs a reasonable approximation to the true texture.



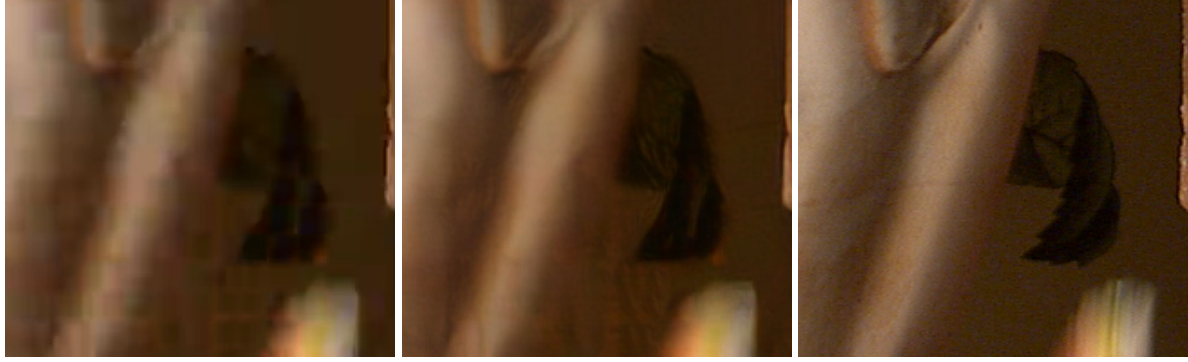


Figure 14. **Compression Artifacts Mistaken for Texture.** Crop from  $1920 \times 1080$  “Cactus”. The compressed image exhibits strong chroma subsampling artifacts (lower right corner). These are mistaken by the GAN as a texture and restored as such.



Figure 15. **Motion Blur.** Crop from  $1920 \times 1080$  “Cactus”. The tiger exhibits high motion which presents itself in the target frame as motion blur. This blur is destroyed by compression and is not able to be restored by the GAN loss. The GAN loss is also “rewarded” for sharp edges which would make reconstructing blurry objects difficult. As an aside, note the additional detail on the background objects in the GAN image when compared to the compressed image.

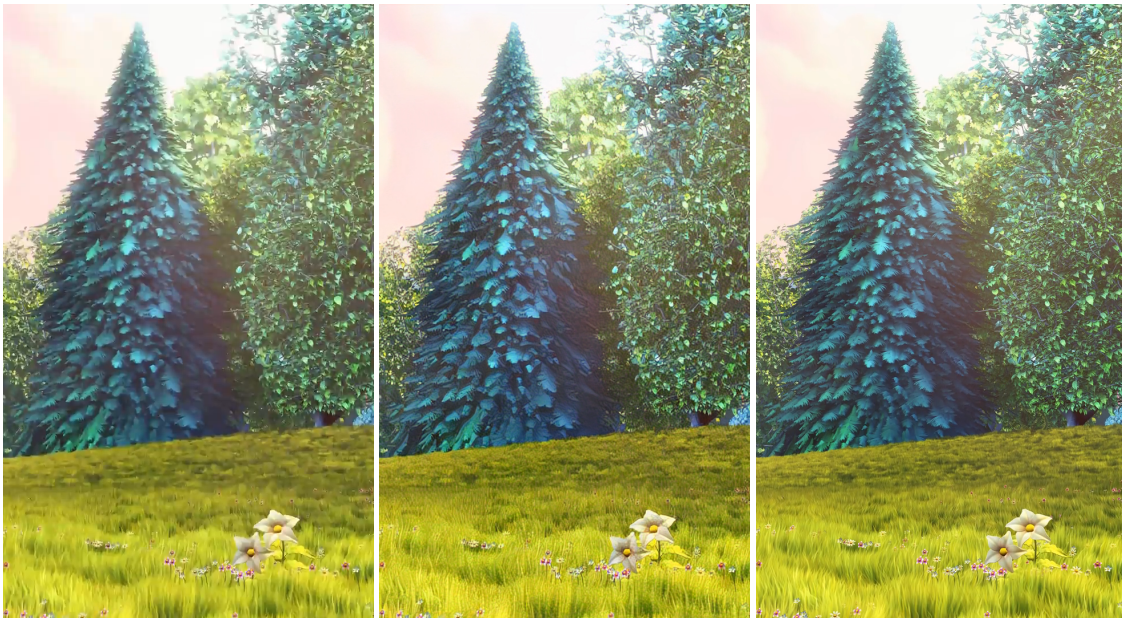


Figure 16. **Artificial.** Crop from  $1920 \times 1080$  “Big Buck Bunny”. This artificial scene is restored accurately despite a lack of artificial training data. Note the grass and tree textures, sharp edges, removal of blocking on the flower, and preservation of the smooth sky region.